Supplementary Information

to the paper " Counterintuitive DNA destabilization by monovalent salt at high concentrations due to overcharging " by Zhang et al.

This PDF file includes:

Figures 1-19
Table 1
Methods 1-6
References

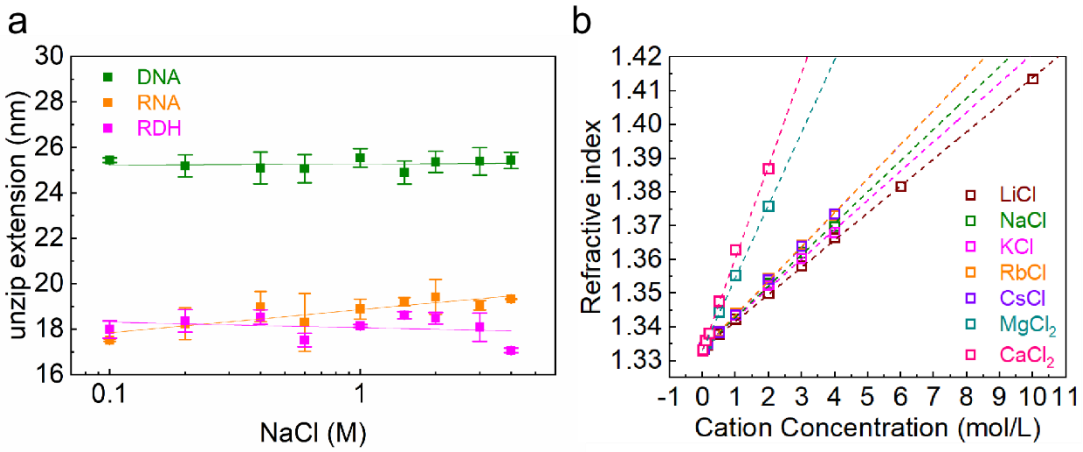

Supplementary Figure 1 | The unfolding length of NA hairpins at various salt concentrations. Source data are provided as a Source Data file. (a) Under equilibrium, we quantified the unfolding lengths (ΔL) of NA hairpins at each salt concentration. The averages and standard errors obtained from three experiments were plotted as data points and error bars. We found ΔL was only slightly affected by salt concentration. We plotted ΔL at various NaCl concentrations as an example. (b) The refractive index of salt solutions at various salt concentrations. The refractive index is measured using refractometer (ATAGO PAL-RI) at 22 °C, 10 mM Tris-HCl (pH 7.5). The dash lines are linear fits for each type of salt.

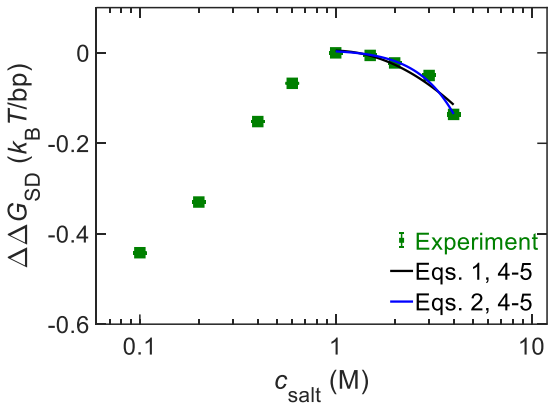

Supplementary Figure 2 | The change of free energy difference between duplex and stretch single-stranded DNA states ($\Delta\Delta G_{SD}$), with the concentration of KCl (c_{salt}). Source data are provided as a Source Data file. The averages and standard errors obtained from three molecules were plotted as data points and error bars (olive). The black curve is similarly obtained from all-atom MD simulation and Eqs. 1, 4-5 and the blue curve from Eqs. 2, 4-5 in the main text.

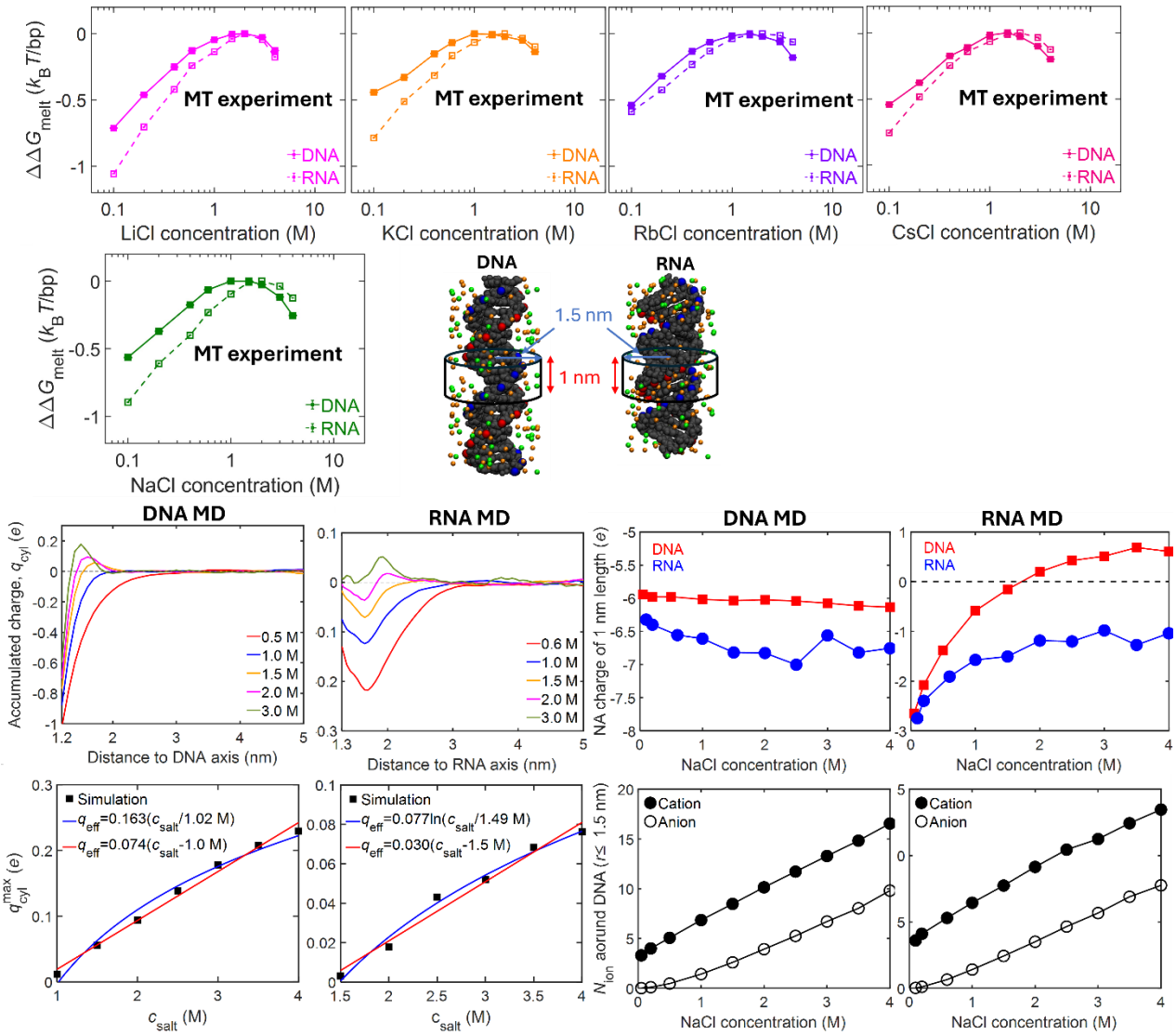

Supplementary Figure 3 | Comparison of RNA and DNA overcharging. Source data are provided as a Source Data file. For MT experiments, the averages and standard errors from four molecules for CsCl and three molecules for other ions are plotted as data points and error bars. $\Delta\Delta G_{\mathrm{SD}}$ is the variance of free energy difference between duplex and stretched ssDNA states. $q_{\mathrm{cyl}}^{\mathrm{max}}$ is the maximum of accumulated charge (q_{cyl}). N_{ion} is the number of ions binding to DNA or RNA duplex over an axis of 1 nm. MT experiments indicate that RNA overcharging requires higher salt concentrations and experiences less destabilization than DNA at equivalent ion concentrations, a difference captured by MD simulations. DNA overcharges at 1 M NaCl, while RNA does so at 1.5 M NaCl, likely due to structural differences such as helical pitch (2.7 nm for RNA vs. 3.4 nm for DNA), radius, and groove structure. Analyzing helical pitch, we found that over a 1 nm axis, DNA holds -6e, and RNA about -7e, depending on salt concentration and nucleic acid deformation. When calculating total ion charge in a 1.5 nm radius, 1 nm height cylinder, we observed +6.5e for DNA (resulting in overcharging, -6e + 6.5e > 0) and +6e for RNA (no overcharging, -7e + 6e < 0).

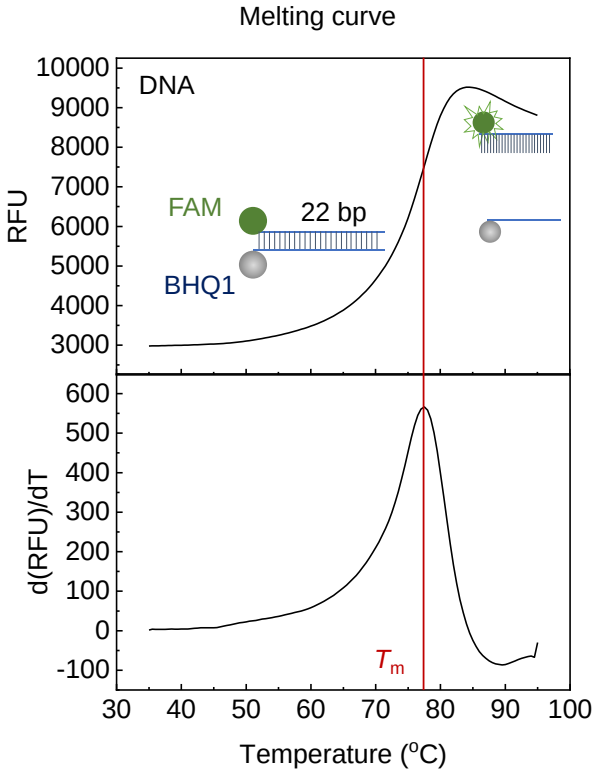

Supplementary Figure 4 | Schematic representation illustrating the measurement of melting temperatures (T_m) for 22 bp short NA duplexes. A representative experiment on DNA duplex at 4 M NaCl is shown. Source data are provided as a Source Data file. We measured the thermal stabilities of NA duplexes using the fluorescence quenching test (FQT), similar to previous works[1]. We designed two complementary paired single-strand NA. One strand was labeled with the FAM group at the 5' end and its complementary strand was labeled with the BHQ1 group at the 3' end. When the two single-stranded oligos were annealed into double-stranded NA, BHQ1 quenched the FAM fluorescence. When the NA duplexes melted during heating up, the fluorescence intensity increased due to the release of the BHQ1 strand. The peak of the derivative of the fluorescence intensity gave T_m. Following are the sequences of oligos used in thermal melting experiments.

DNA_FAM: FAM-GACGATCGTTCGTGAAGTCAAC

DNA_BHQ1: GTTGACTTCACGAACGATCGTG-BHQ1

RNA_FAM:

FAM-/rG/rA/rC/rG/rA/rU/rC/rG/rU/rU/rC/rG/rU/rG/rA/rA/rG/rU/rC/rA/rA/rC/

RNA_BHQ1:

BHQ1-/rG/rU/rU/rG/rA/rC/rU/rU/rC/rA/rC/rG/rA/rA/rC/rG/rA/rU/rC/rG/rU/rG/

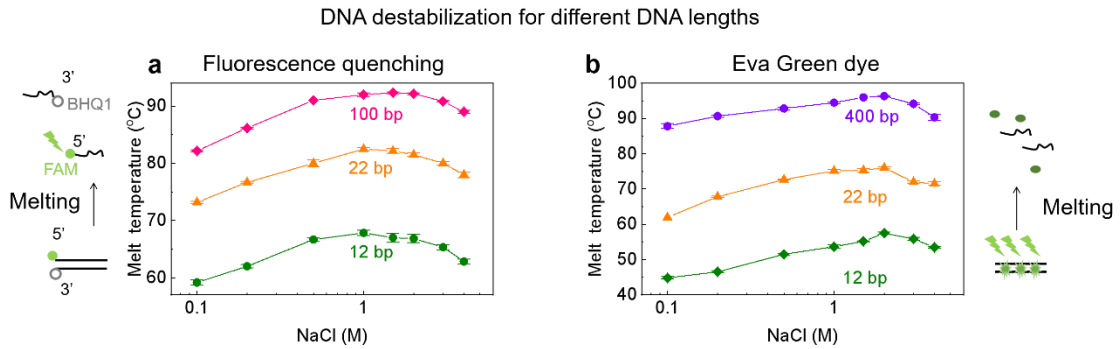

Supplementary Figure 5 | Melting temperatures (T_m) for different DNA lengths. Source data are provided as a Source Data file. (a) Effects of NaCl concentration on T_m measured by fluorescence quenching test. The averages and standard errors from several experiments (six for 22 bp and three for other lengths) are plotted as data points and error bars. (b) Effects of NaCl concentration on T_m measured by double-stranded DNA dye (Eva Green). The averages and standard errors from three experiments are plotted as data points and error bars. We obtained 400 bp dsDNA by PCR using DNA400_F and DNA400_R as primers and lambda DNA as template. The sequence of 22 bp DNA is included in the main text and the following are the sequences of oligos used in thermal melting experiments here.

DNA12_FAM: FAM- GACGATCGTTCG
DNA12_BHQ1: CGAACGATCGTC-BHQ1

DNA100_FAM:
FAM-GACGATCGTTCGTGAAGTCAACTTTGCATGAGAGAATTTGTACCACCTCCCACC
GACCATCTATGACTGTACGCCACTGTCCCTAGGACTGCTATGTGCT
DNA100_BHQ1:
AGCACATAGCAGTCCTAGGGACAGTGGCGTACAGTCATAGATGGTCGGTGGGAGGT
GGTACAAATTCTCTCATGCAAAGTTGACTTCACGAACGATCGTC-BHQ1

DNA12: GACGATCGTTCG
DNA12: CGAACGATCGTC

DNA400_F: CGCCAAAGGAGATTATGTAC
DNA400_R: GGTGCGTTTCGTTGGAAG

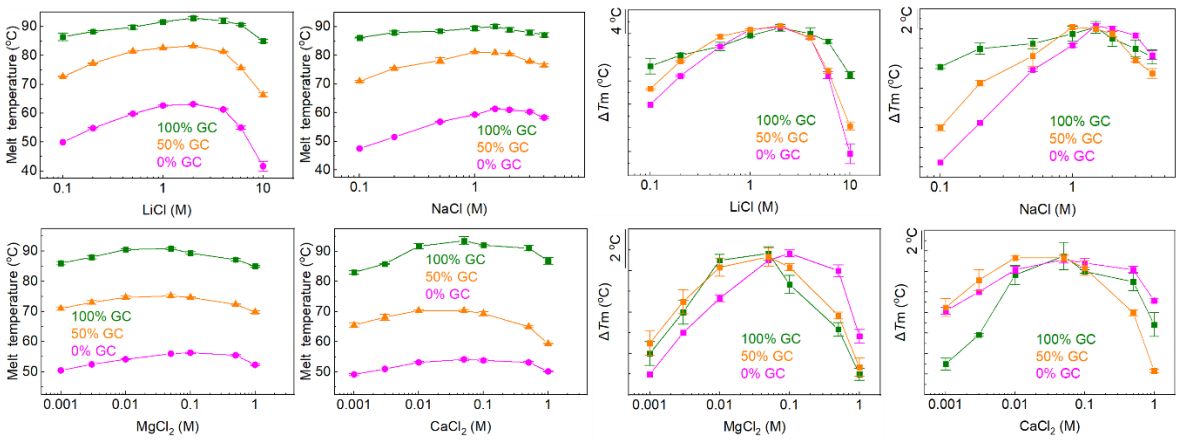

Supplementary Figure 6 | Comparison of melting temperatures (T_m) for three DNA sequences with 100% GC, 50% GC, and 0% GC. The averages and standard errors from several experiments (six for 50% GC and three for others) are plotted as data points and error bars. Source data are provided as a Source Data file. Sequences are GCGGCGCCCGCGCCCGCGGCGC, GACGATCGTTCGTGAAGTCAAC, and TATTATAAATATAAATATTATA, respectively. The left panel shows the original T_m, while the right panel shows the changes in T_m (ΔT_m). Because a GC pair contains three hydrogen bonds while an AT pair contains two hydrogen bonds. If hydrogen bonds play a leading role in DNA destabilization, the slopes of the c_{salt}- T_m curves around c^*_{salt} for 100% GC should be larger than the ones with 50% and 0% GC. Here, c^*_{salt} represents a critical salt concentration where T_m reaches a peak. The figure shows that there are some variations in the slopes among three sequences. However, there is no trend when varying the GC content. Especially, in the case of NaCl, the DNA with 100% GC has the smallest slope. These results suggest hydrogen bonds may not be the leading reason for DNA destabilization by monovalent ions.

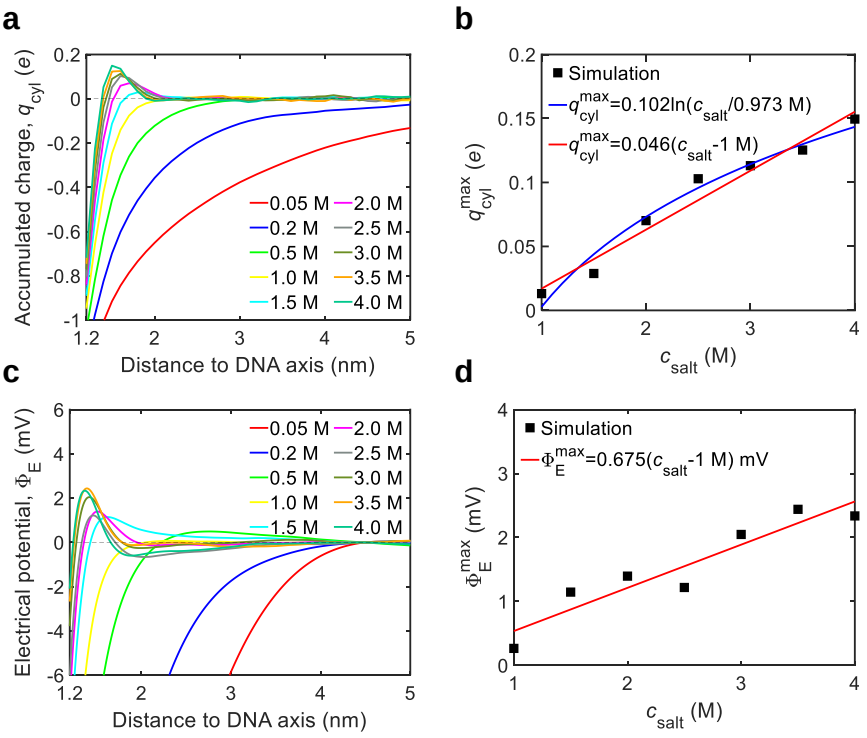

Supplementary Figure 7 | Ion distribution of K^+ around DNA duplex from all-atom MD simulations. Source data are provided as a Source Data file. c_{salt} is salt concentration. (a) Accumulated charge, q_{cyl}, as a function of the cylindrical radius. (b) Maximum of q_{cyl} as a function of KCl concentration. (c) Electric potential, Φ_{E}, as a function of radial distance. (d) Maximum of Φ_{E} as a function of KCl concentration.

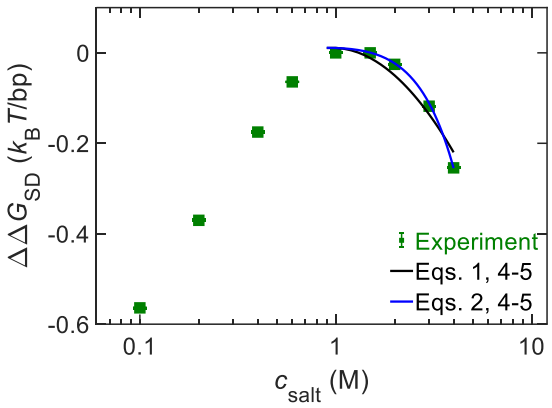

Supplementary Figure 8 | The change of free energy difference between duplex and stretch single-stranded DNA states ($\Delta\Delta G_{SD}$), with the concentration of CsCl (c_{salt}). Source data are provided as a Source Data file. The averages and standard errors obtained from four molecules were plotted as data points and error bars. The black curve is similarly obtained from all-atom MD simulation and Eqs. 1, 4-5 and the blue curve from Eqs. 2, 4-5 in the main text.

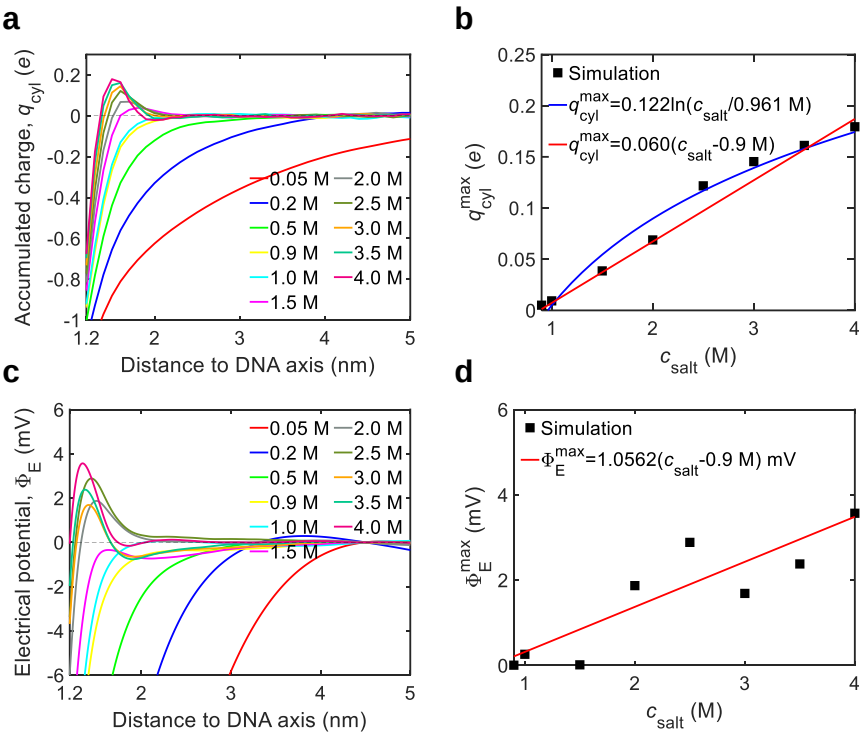

Supplementary Figure 9 | Ion distribution of Cs^+ around DNA duplex from all-atom MD simulations. Source data are provided as a Source Data file. (a) Accumulated charge, q_{cyl}, as a function of the cylindrical radius. (b) Maximum of q_{cyl} as a function of CsCl concentration. (c) Electric potential, Φ_{E}, as a function of radial distance. (d) Maximum of Φ_{E} as a function of CsCl concentration.

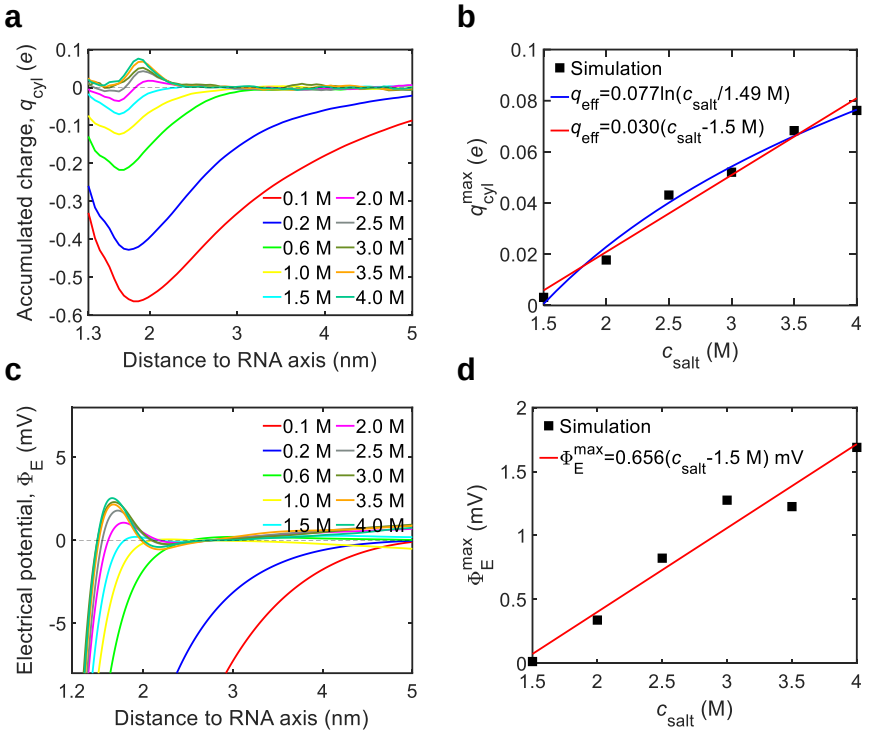

Supplementary Figure 10 | Ion distribution of Na^+ around RNA duplex from all-atom MD simulations. Source data are provided as a Source Data file. (a) Accumulated charge, q_{cyl}, as a function of the cylindrical radius. (b) Maximum of q_{cyl} as a function of NaCl concentration. (c) Electric potential, Φ_{E}, as a function of radial distance. (d) Maximum of Φ_{E} as a function of NaCl concentration.

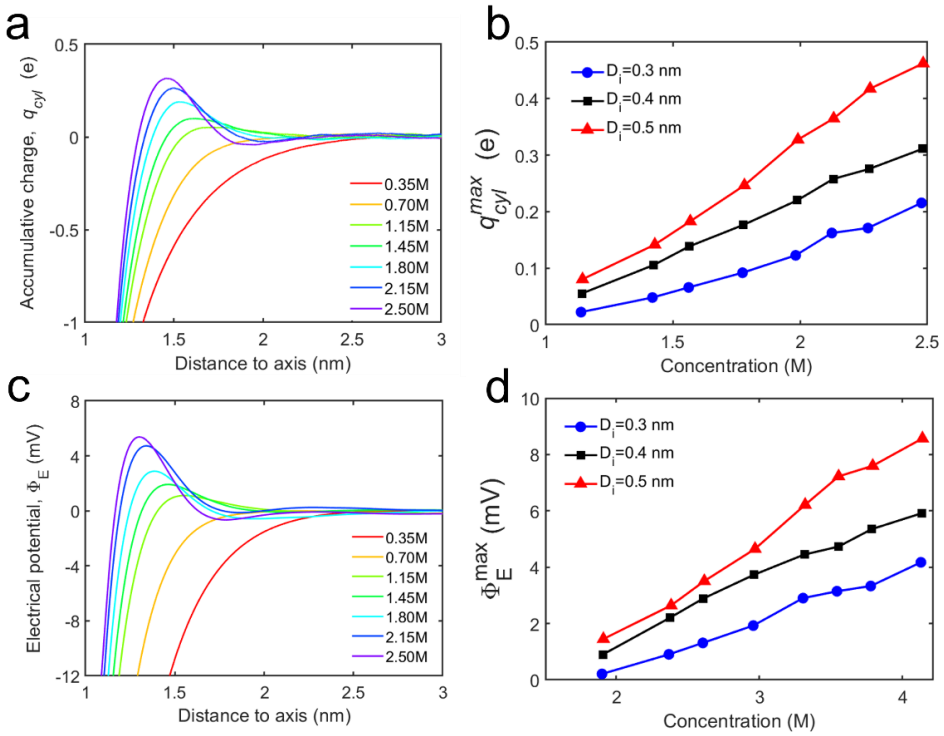

Supplementary Figure 11 | Monovalent ion distribution around DNA duplex from coarse-grained Langevin dynamics simulations using LAMMPS. Source data are provided as a Source Data file. (a) Accumulated charge, q_{cyl}, as a function of the cylindrical radius. (b) Maximum of q_{cyl}, $q_{\mathrm{cyl}}^{\mathrm{max}}$, as a function of salt concentration. (c) Electric potential, Φ_{E}, as a function of radial distance. (d) Maximum of Φ_{E}, $\Phi_{\mathrm{E}}^{\mathrm{max}}$, as a function of salt concentration. In (a) and (c), Ions are modelled as hard spheres with the diameters $D_i = 0.4$ nm.

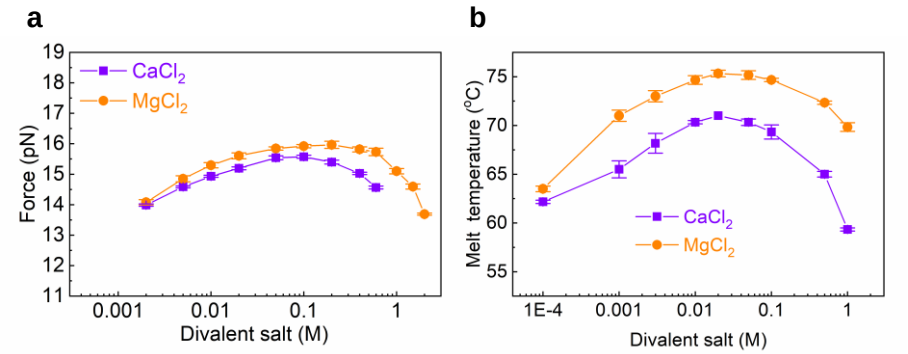

Supplementary Figure 12 | Measurement of DNA duplex stability with divalent salts. The averages and standard errors from three experiments were plot as data points and error bars. Source data are provided as a Source Data file. (a) Equilibrium force as functions of salt concentrations measured in MT experiments. (b) The melting temperatures as functions of salt concentrations measured in fluorescence quenching tests.

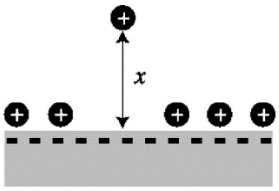

Supplementary Figure 13 | Attraction between an additional counterion and already neutralized surface. This additional counterion creates its negative correlation hole. Duplicated from Figure 6 in[2]. In the mean-field treatment, when DNA negative charges are fully compensated by counterions, DNA has no attraction with additional counterions. The mean-field treatment assumes counterions distribute continuously on DNA charged surface. However, in the real case, counterions are discrete particles. When counterions strongly repel each other, they form a crystal-like structure on the surface. Under such a situation, the additional counterion produces a hole on DNA surface, which significantly reduces the counterion-counterion repulsion. Then, the total interaction of the additional counterions with DNA and existing counterions becomes attractive (see the figure below). This attraction corresponds to μ in Eq. S8. DNA can keep absorbing additional counterions until the Boltzmann distribution of counterions, $\exp(-\mu/k_BT)$, is satisfied, which causes DNA overcharging.

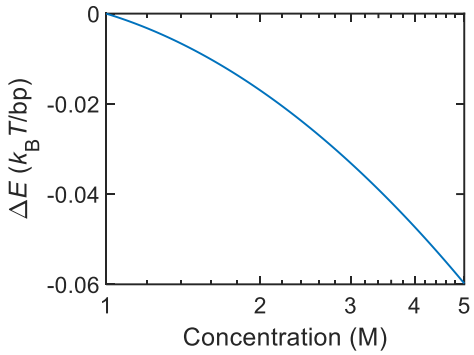

Supplementary Figure 14 | DNA destabilization by high salt concentration. Source data are provided as a Source Data file. The result is calculated using the model by Maity, Singh, and Singh (2017)[3].

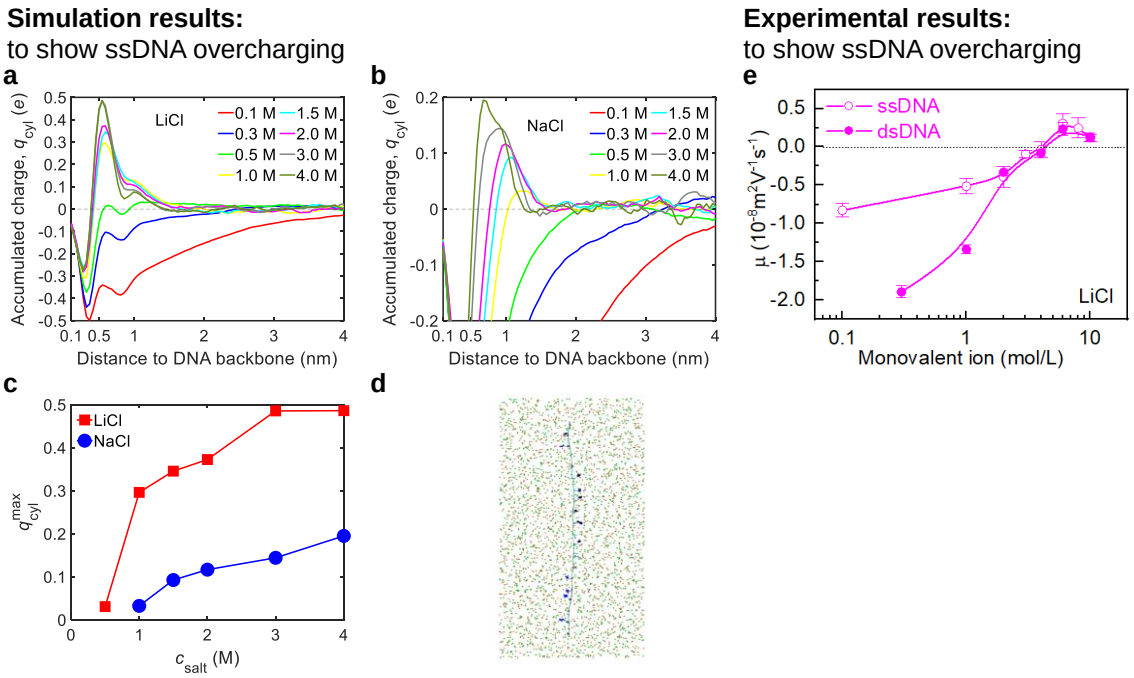

Supplementary Figure 15 | Simulation and electrophoresis experiments of ssDNA overcharging. Source data are provided as a Source Data file. In simulation results, the accumulated charge, q_{cyl}, as a function of the distance to ssDNA backbone for simulations at (a) LiCl or (b) NaCl indicate ssDNA overcharging, along with (c) the maximum of q_{cyl}, $q_{\mathrm{cyl}}^{\mathrm{max}}$, as a function of salt concentrations. (d) The ssDNA simulation system is illustrated for clarity. In electrophoresis experiments, (e) the electrophoretic direction of ssDNA/dsDNA is reversed at high concentrations of LiCl. Positive values of μ correspond to DNA migrating toward the cathode. We performed experiments using M13 single-stranded DNA plasmid and 8 kbp dsDNA by PCR. The error bars represent the standard errors among three independent experiments. We performed all-atoms molecular dynamics simulations to validate whether overcharging occurs for ssDNA. A stretched 20-nt ssDNA with the sequence of CGACTCTACGGCATCTGCGC was immersed in a $10 \times 10 \times 18\ \mathrm{nm}^3$ simulation box containing TIP3P water molecules. The ssDNA molecule is kept in stretched straight form, in consistence with the unzipping conformation from the MT experiments. All simulation parameters are similar to that of dsDNA overcharging. As shown in simulation results, DNA overcharges around 0.6 nm to the backbone upon NaCl concentrations increases to 1 M or LiCl concentration reaches 0.5 M. Our experimental results of electrophoretic mobility also indicate ssDNA overcharging.

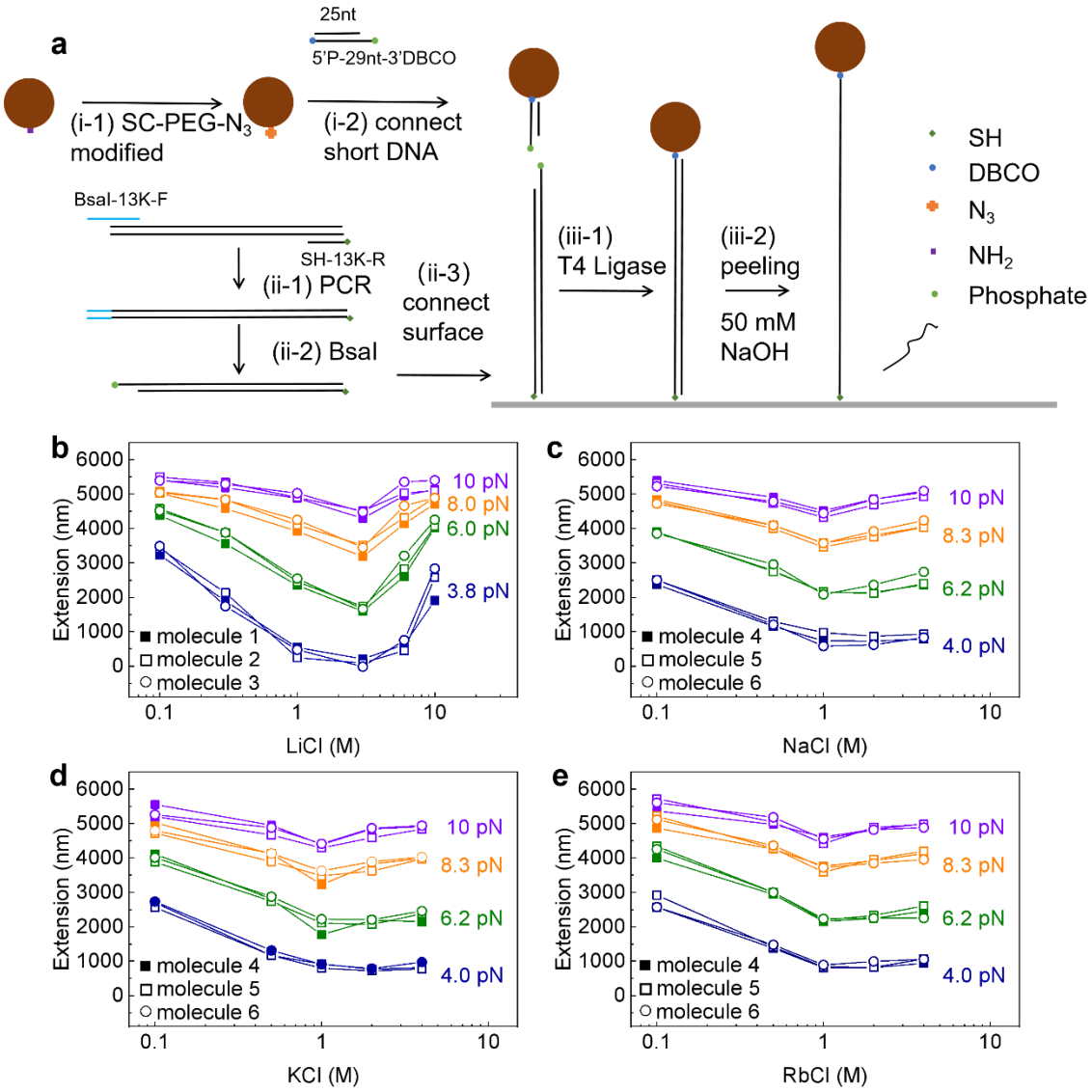

Supplementary Figure 16 | Extension of single-stranded DNA (ssDNA) vs salt concentration indicates overcharging. Source data are provided as a Source Data file. Through MT experiments using 13751-nt ssDNA, we observed that the extension of ssDNA reversed at high concentrations of monovalent ions under constant forces, possibly due to charge reversion of the ssDNA. Under a constant force, the extension of ssDNA decreased with increasing salt concentration, likely due to the neutralization of its negative charge. However, at concentrations exceeding a threshold, the extension of ssDNA increased with increasing salt concentration, which may be attributed to charge reversion and the resulting increased repulsion between the net positive charges of the ssDNA.

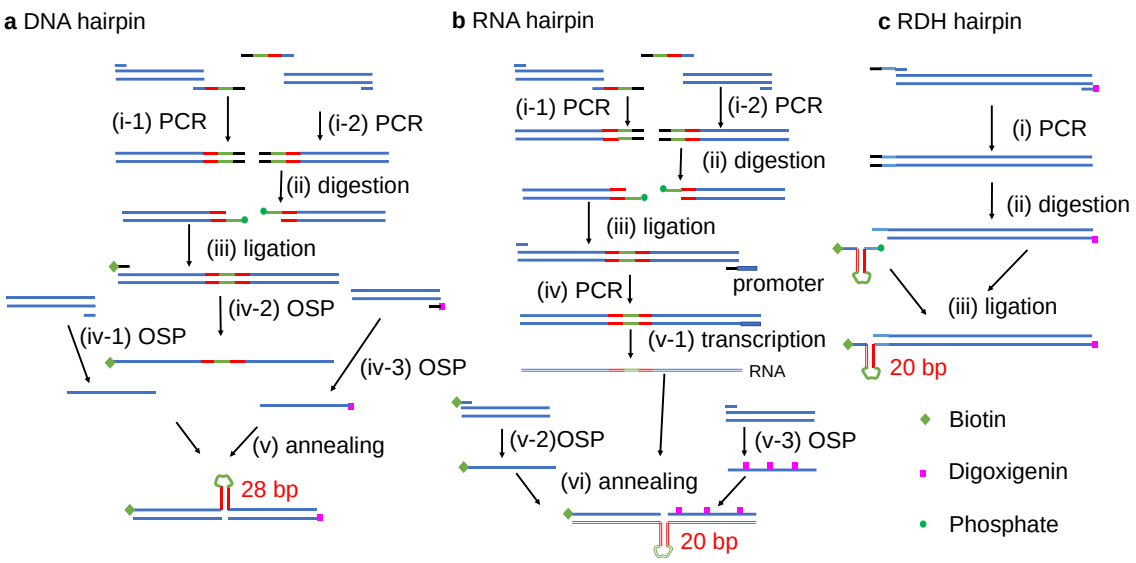

Supplementary Figure 17 | Flowchart to prepare the DNA, RNA, and RDH hairpins for magnetic tweezers (MT) experiments. (a) The DNA hairpin construct. (b) The RNA hairpin construct. (c) The RDH hairpin construct.

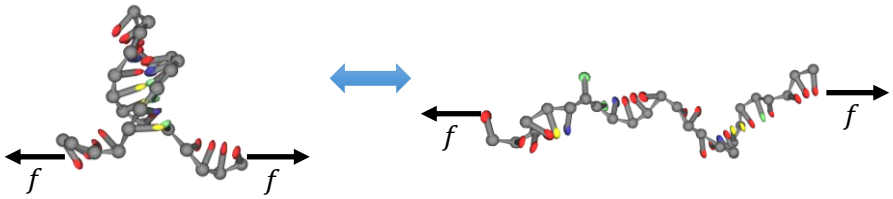

Supplementary Figure 18 | Illustration of transition between DNA. (a) folded and (b) stretched state using the oxDNA model under stretching force. Two DNA images were from our simulation snapshots.

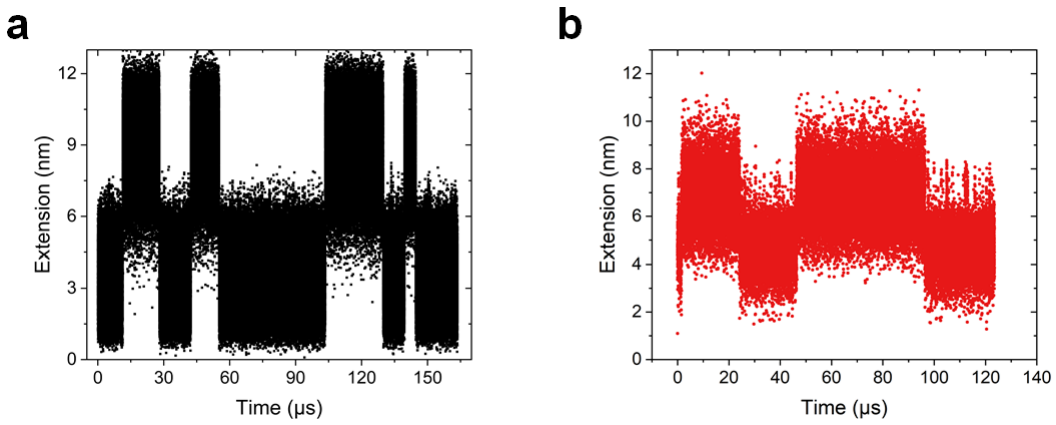

Supplementary Figure 19 | DNA and RNA extension as a function of the simulation time. Source data are provided as a Source Data file. The two-state feature of (a) DNA or (b) RNA extension indicates the unfolding and refolding of a DNA or RNA hairpin.

Supplementary Table 1 | The determined Eqs. 1-3, 5 for different monovalent ions on DNA.

DNA	Eq. 1	Eq. 2	Eq. 3	Eq. 5
NaCl	$q_{\mathrm{cyl}}^{\max} \approx 0.163 \ln(c_{\mathrm{salt}}/1.02\ \mathrm{M})$	$q_{\mathrm{cyl}}^{\max} \approx 0.074(c_{\mathrm{salt}} - 1\ \mathrm{M})$	$\Phi_{\mathrm{E}}^{\max} \approx 1.509(c_{\mathrm{salt}} - 1\ \mathrm{M})$	$E_{\mathrm{elec}} \approx 1.4E_0$
KCl	$q_{\mathrm{cyl}}^{\max} \approx 0.102 \ln(c_{\mathrm{salt}}/0.97\ \mathrm{M})$	$q_{\mathrm{cyl}}^{\max} \approx 0.046(c_{\mathrm{salt}} - 1\ \mathrm{M})$	$\Phi_{\mathrm{E}}^{\max} \approx 0.675(c_{\mathrm{salt}} - 1\ \mathrm{M})$	$E_{\mathrm{elec}} \approx 1.7E_0$
CsCl	$q_{\mathrm{cyl}}^{\max} = 0.122 \ln(c_{\mathrm{salt}}/0.96\ \mathrm{M})$	$q_{\mathrm{cyl}}^{\max} \approx 0.060(c_{\mathrm{salt}} - 0.9\ \mathrm{M})$	$\Phi_{\mathrm{E}}^{\max} \approx 1.056(c_{\mathrm{salt}} - 0.9\ \mathrm{M})$	$E_{\mathrm{elec}} \approx 1.6E_0$

Supplementary Method 1: Calculating ΔG_{CD} between the coil and duplex states

The free energy difference between the coil state and the duplex state, ΔG_{CD}, at room temperature (22 °C) can be estimated using the nearest-neighbor model[4], which gives the enthalpy change and entropy change: ΔH and ΔS. One can calculate ΔG_{CD} using the equation:

$$\Delta G_{\mathrm{CD}} = \Delta H - T\Delta S$$

where T is the temperature. The sequence of stem region in DNA hairpin is 5'-TAGAC-GATCG-TTCGT-GAAGT-CAACA-TCG-3'. In this model, we first counted the numbers of stacking (adjacent base pairs) in different types, and then multiplied these numbers with the relevant enthalpy changes and entropy changes. Finally, we add these values:

$$\begin{aligned}\Delta G_{\mathrm{CD}}^{\mathrm{chain}} = {} & 3\Delta G_{\mathrm{CD}}(\mathrm{AA/TT}) + 2\Delta G_{\mathrm{CD}}(\mathrm{AT/TA}) + \Delta G_{\mathrm{CD}}(\mathrm{TA/AT}) + 3\Delta G_{\mathrm{CD}}(\mathrm{CA/GT}) + \\ & 5\Delta G_{\mathrm{CD}}(\mathrm{GT/CA}) + 2\Delta G_{\mathrm{CD}}(\mathrm{CT/GA}) + 7\Delta G_{\mathrm{CD}}(\mathrm{GA/CT}) + 4\Delta G_{\mathrm{CD}}(\mathrm{CG/GC}) + \\ & \Delta\Delta G_{\mathrm{CD}}(\mathrm{init.}) = -190.74\ \mathrm{kJ/mol}\end{aligned}$$

We averaged the above value over 28 bp:

$$\Delta G_{\mathrm{CD}} = \Delta G_{\mathrm{CD}}^{\mathrm{chain}}/28 = -2.77\ k_{\mathrm{B}}T/\mathrm{bp}.$$

Supplementary Method 2: DNA overcharging using the theory by Shklovskii et al.

Shklovskii et al. derived the condition of DNA overcharging based on the Wigner-crystal treatment of counterions[2, 5]. They obtained the linear charge density of DNA and ions as:

$$\eta^* = \eta \frac{\ln(c_{\text{salt}}/c_0)}{\ln[4/(\pi c_{\text{salt}} l_B^3)]}$$

where $\eta \equiv k_B T \times 4\pi\epsilon\epsilon_0/e \approx 1.41\ e/\text{nm}$, e is the electron charge, and $l_B = e^2/(4\pi\epsilon\epsilon_0 k_B T) \approx 0.707\ \text{nm}$ is the Bjerrum length. The above equation is adapted from Eq. 15 in [2]. Here, c_0 is the critical monovalent salt concentration, which can be calculated by the following equations:

$$c_0 = \frac{\sigma}{0.3\ \text{nm} \times e} \exp(-\frac{\mu}{k_B T})$$

$$\sigma = e/(2\pi \times 1\text{nm} \times 0.17\text{nm})$$

$$\mu = -k_{\text{B}} T\left(1.65\Gamma - 2.61\Gamma^{1/4} + 0.26 \ln \Gamma + 1.81\right)$$

$$\Gamma = 1.76 \frac{\sqrt{\sigma/e}e^2}{4\pi\epsilon\epsilon_0}$$

where σ is DNA surface charge density, $\Gamma \approx 1.21$, and $\mu \approx -1.12\ k_B T$. Eventually, $c_0 \approx 1.69$ M. In σ, 1 nm is the DNA radius and 0.17 is the distance between two charges along the DNA axis. The expression of c_0 and μ are adapted from Eq. 10 and Eq. 7 in [6], respectively. Γ is adapted from Eq. 3 and Eq. 4 in [6], and the coefficient 1.76 is the multiplication of the two coefficients of 1.96 and 0.9.

In our work, $q_{\text{cyl}}^{\max}$ is defined as the excessive charge per base pair, i.e. per 0.34 nm. Hence, we adapt Eq. 1 to

$$q_{\text{cyl}}^{\max} = 0.34\ \text{nm} \times 1.41 \frac{e}{\text{nm}} \frac{\ln(c_{\text{salt}}/c_0)}{\ln[4/(\pi c_{\text{salt}} l_B^3)]} = 0.48e \times \frac{\ln(c_{\text{salt}}/1.69\ \text{M})}{\ln(6\ \text{M}/c_{\text{salt}})}.$$

In the above equations, the two quantities 1.69 M and 6 M appear to deviate from our all-atom simulation results in Fig. 4c. There are several reasons. First, the theory by Shklovskii et al. was originally developed for multivalent counterions, where counterion-counterion repulsion is strong. Here, we deal with monovalent counterions. Second, many approximations are made when deriving equations. If we treat these two quantities as fitting parameters, we obtain:

$$q_{\text{cyl}}^{\max} = 0.48e \times \frac{\ln(c_{\text{salt}}/1\ \text{M})}{\ln(105\ \text{M}/c_{\text{salt}})}.$$

Inspired by our simulation results in Fig. 4c, we approximate the above equation by

$$q_{\mathrm{cyl}}^{\max} = 0.163e \times \ln[c_{\mathrm{salt}}\,/(1\ \mathrm{M})]\ ,$$

As shown in Fig. 4c, the above equation is numerically close to a linear relationship over the range of $1\ \mathrm{M} \le c_{salt} \le 4\ \mathrm{M}$:

$$q_{\mathrm{cyl}}^{\max} \approx 0.074(c_{\mathrm{salt}} - 1\ \mathrm{M})\ .$$

For convenience, we will use the linear equation to derive the overcharging electrical potential.

Based on $q_{\mathrm{cyl}}^{\max}$, we can derive $\Phi_E^{\max}$. Using the Gauss's law, the excessive charges produce an electric field:

$$E = q_{\mathrm{cyl}}^{\max}/(2\pi \times 1\mathrm{nm} \times 0.34\ \mathrm{nm} \times 4\pi\epsilon\epsilon_0)\ .$$

Based on the theory by Shklovskii et al., the thickness of the overcharging layer is about $l_B \approx 0.71\ \mathrm{nm}$. Supposing the electric field linearly decay to zero over this thickness, combining above two formulas of $q_{\mathrm{cyl}}^{\max}$ and E yields the electric potential for DNA overcharging:

$$\Phi_E^{\max} = El_B/2 \approx 2.13(c_{\mathrm{salt}} - 1\ \mathrm{M})\ \ [\text{ in unit of mV}].$$

Supplementary Method 3: Coarse-grained Langevin dynamics simulations

The coarse-grained Langevin dynamics simulations were performed using the LAMMPS 2020 simulation package[7]. The pairwise interactions between particles were described by Lennard-Jones potential:

$$V_{\mathrm{LJ}}(r) = 4\epsilon\left[\left(\frac{\sigma}{r}\right)^{12} - \left(\frac{\sigma}{r}\right)^{6}\right].$$

We set $\epsilon = 4\ k_{\mathrm{B}}T$. The value of σ was set as the sum of the radii of two particles in this interaction. The cutoff distance of LJ interaction is $2^{1/6}\sigma$. The electrostatic interactions were calculated in real space with a cutoff of 2.5 nm using pairwise Coulombic potential. The Ewald K-space solver was used for long-range Coulombic interaction. The relative dielectric constant of water in simulations was set to 80. All simulations were carried out in the NVT ensemble with the Langevin thermostat at 295 K. After the simulation reached equilibrium, we collected the data from production runs of 5×10^7 steps to calculate the ion distribution profiles.

We also calculated the electric potential around DNA using the Poisson equation:

$$\nabla^2\psi(r,\theta) = -\frac{\rho_e}{\epsilon}.$$

To analyze the role of the excluded volume interaction of ions in DNA overcharging, we define a quantity $c_{\mathrm{salt}}D_i^2$, where c_{salt} is the salt concentration and D_i is the ion diameter. Figure 5g shows Φ_E^{max} versus $c_{\mathrm{salt}}D_i^2$. The simulation results from different ion radius collapse, indicating a leading role of the excluded volume interaction of ions in DNA overcharging.

Supplementary Method 4: Comparison with Maity, Singh and Singh (2017)

Maity, Singh and Singh used a modified Peyrard Bishop Dauxois (PBD) model to capture DNA destabilization by high salt concentrations[3]. Here, we re-calculated the DNA energy change at high salt concentrations in their model. The dissociation energy of one base-pair follows**:**

$$V = V_m(y_i) + V_{sol}(y_i)$$
$$V_m(y_i) = D_i(e^{-a_i y_i} - 1)^2$$
$$V_{sol} = -\frac{1}{4}D_i[\tanh(\gamma y_i) - 1]$$
$$D_i = D_0\left(1 + \lambda_1 \ln\frac{C}{C_0} - \lambda_2 \ln^2\left(\frac{C}{C_0}\right) + \chi\left(\frac{C_0}{C^t}\right)\right)$$

where y_i is the base-base distance with $y_i = 0$ corresponding to the minimum energy, D_i is the interaction strength, C is the monovalent salt concentration and C_0 is the critical salt concentration. Other parameters are $D_0 = 0.043\ eV$, $\lambda_1 = 0.01$, $\lambda_2 = 0.011$, $C_0 = 1\ \mathrm{M}$, $\chi = 1.2$ and $t = 0.01$. DNA melting corresponds to the change of y_i is from 0 to ∞. Accordingly, we have $\Delta V \approx \frac{3}{4}D_i$. DNA destabilization is related to the terms $\lambda_2 \ln^2\left(\frac{C}{C_0}\right) + \chi\left(\frac{C_0}{C^t}\right)$ in the above equations. Hence, we calculate the magnitude of destabilization as

$$\Delta E = -\frac{3}{4}D_0\left(\lambda_2 \ln^2\left(\frac{C}{C_0}\right) - \chi\left(\frac{C_0}{C^t}\right)\right)$$

Supplementary Method 5: Preparation of ssDNA for MT experiments

We prepared the ssDNA for MT experiments by following steps:

(i-1) We use SC-PEG-N_3 to modify the magnetic beads of the amino surface

(i-2) We anneal 5'P-29nt-3'DBCO and 25nt in a 1:1 ratio to generate 4-base 5' sticky ends. The magnetic beads of the N3 surface are reacted to the short dsDNA fragment with the DBCO group.

(ii-1) Prepare a DNA fragment by PCR using BsaI-13K-F and SH-13K-R as primers and lambda DNA as the template.

(ii-2) The PCR products were digested with the restriction enzyme BsaI (NEB #R3733) at 37°C for 1 hour to generate 4-base 5' sticky ends.

(ii-3) The thiol end of dsDNA was connected to the surface of the channel.

(iii-1) The magnetic beads with short dsDNA fragment and the long dsDNA fragment were ligated using T4 DNA ligase (Thermo Scientific™, EL0014).

(iii-2) We used 50 mm NaOH peeling dsDNA to get the single-stranded DNA of the surface and magnetic beads

The sequences used to prepare NA hairpin constructs are as follows.

BsaI-13K-F:	CGATCGGTCTCATCAGGCTTGGCTCTGCTAACACGTTGC TCATAGGAG
SH-13K-R:	/5'SH/AGTCAGTTGCATCAGTCACAAGGG
25nt:	AGACTTCCAAAGAATCTCGTTCTGC
5'P-29nt-3'DBCO:	/5'P/ CTGAGCAGAACGAGATTCTTTGGAAGTCT/3'DBCO/

Supplementary Method 6: Preparation of hairpins for MT experiments

The DNA hairpin construct.

(i-1) Prepare a short DNA fragment by PCR using 13K_F and HD_DNAh_R_bsai as primers and lambda DNA as the template.

(i-2) Another PCR was performed using HD_DNAh_F_bsai and 13K_R as primers and lambda DNA as the template.

(ii) The two PCR products were digested with the restriction enzyme BsaI (NEB #R3733) at 37°C for 1 hour to generate 4-base 5' sticky ends.

(iii) The two digested products were ligated in a 1:1 ratio using T4 DNA ligase (Thermo Scientific™, EL0014). Gel purification was performed to obtain the ligated product.

(iv-1) A ssDNA strand was amplified by one-sided PCR (OSP) using HD_R as the primer and the PCR product obtained in step (i-1) as the template.

(iv-2) A ssDNA labeled with biotin was amplified by OSP using 13K_FB as the primer and the ligated product in step (iii) as the template.

(iv-3) A ssDNA labeled with digoxigenin was amplified by OSP using 13K_RD as primer, and PCR production was obtained in step (i-2) as the template.

(v) Annealing the three ssDNA obtained in step (iv) together equimolar through a temperature process containing a one-hour incubation step at 65 °C followed by an slow cooling process from 65 °C to 25 °C (-0.5 °C /min).

The RNA hairpin construct.

(i-1) PCR was performed using 13K_F and HD_RNAh_R_bsai as primers and lambda DNA as the template.

(i-2) Another PCR was performed using HD_RNAh_F_bsai and 13K_R as primers and lambda DNA as the template.

(ii) The two PCR products were digested with the restriction enzyme BsaI at 37°C for 1 hour to generate 4-base 5' sticky ends.

(iii) The two digested products were ligated in a 1:1 ratio using T4 DNA ligase (Thermo Scientific™, EL0014). Gel purification was performed to obtain the ligated product.

(iv) PCR was performed using 13K_F and HD_R as primers and lambda DNA as the template. Similarly, another PCR was performed using HD_F and 13K_R as primers and lambda DNA as the template.

(v-1) The long ssRNA strand was generated using the ligated production obtained in step (iii) by T7 RNA polymerase.

(v-2) A ssDNA labeled with biotin was generated by OSP using 13K_FB as the primer and the PCR product obtained in step (i) as the template.

(v-3) A multiple-digoxigenin-labeled ssDNA was generated by OSP using HD_F as the primer and the PCR product obtained in step (i) as the template together with 30% Digoxigenin-dUTP (Roche).

(vi) Annealing the two ssDNA and one ssRNA together equimolar through a temperature process containing a one-hour incubation step at 65 °C followed by a slow cooling process from 65 °C to 25 °C (-0.5 °C /min).

The RDH hairpin construct.

(i) PCR was performed using 13K_RD and HD_F_bsai as primers and lambda DNA as the template.

(ii) The PCR product obtained in step (i) was digested by the restriction enzyme BsaI at 37°C for 1 hour to generate a 4-base 5' sticky end.

(iii) Ligating the synthesized RDH_hairpin to the digested product using T4 DNA ligase. Gel purification was performed to obtain correct ligated product.

The sequences used to prepare NA hairpin constructs are as follows.

13K_F:	ATTTACGCCGGGATATGTCAAGC
13K_R:	AGTCAGTTGCATCAGTCACAAGGG
13K_FB:	/5'bio/ATTTACGCCGGGATATGTCAAGC
13K_RD:	/5'Dig/AGTCAGTTGCATCAGTCACAAGGG
HD_R:	TAGCCGCTGGCCACCATACTGG
HD_1F:	ATGTGGTGATGCCGGATGA
HD_F_bsai:	CCAGGGTCTCCGCTG ATGTGGTGATGCCGGATGA
HD_DNAh_R_bsai:	CAGGGTCTCCCACAAACGATGTTGACTTCACGAACGATCGTCTATAGCCGCTGGCCACCATACTG
HD_DNAh_F_bsai:	CAGGGTCTCCTGTGTTCGATGTTGACTTCACGAACGATCGTCTAATGTGGTGATGCCGGATGA
13K_R_P:	TAATACGACTCACTATAGGGAGTCAGTTGCATCAGTCACAAGGG
HD_RNAh_R_bsai:	CCAGGGTCTCCTTTTCGATGTTGACTTCACGAACGTAGCCGCTGGCCACCATACTG
HD_RNAh_F_bsai:	CCAGGGTCTCCAAAACGATGTTGACTTCACGAACGAATGTGGTGATGCCGGATGA
RDH_hairpin:	5'phos/CAGCTCTGT/rG//rA//rC//rU//rC//rG//rU//rU//rC//rA//rG//rU//rC//rA//rA//rC//rA//rU//rC//rG/TTTGTGTTCGATGTTGACTGAACGAGTCTGCATTCG/3'bio/

The sequences of NA hairpins are shown as follows, where the stem region bases are underlined.

DNA_hairpin:
TAGACGATCGTTCGTGAAGTCAACATCGTTTGTGTTCGATGTTGACTTCACGAACGATCGTCTA

RNA_hairpin: CGUUCGUGAAGUCAACAUCGUUUUCGAUGUUGACUUCACGAACG

RDH_hairpin: GACUCGUUCAGUCAACAUCGTTTGTGTTCGATGTTGACTGAACGAGTC

Supplementary References

1. You Y, Tataurov AV, Owczarzy R. Measuring thermodynamic details of DNA hybridization using fluorescence. *Biopolymers* **95**, 472-486 (2011).

2. Grosberg AY, Nguyen TT, Shklovskii BI. Colloquium: The physics of charge inversion in chemical and biological systems. *Reviews of Modern Physics* **74**, 329-345 (2002).

3. Maity A, Singh A, Singh N. Differential stability of DNA based on salt concentration. *European Biophysics Journal* **46**, 33-40 (2017).

4. SantaLucia J. A unified view of polymer, dumbbell, and oligonucleotide DNA nearest-neighbor thermodynamics. *Proceedings of the National Academy of Sciences* **95**, 1460-1465 (1998).

5. Shklovskii BI. Wigner Crystal Model of Counterion Induced Bundle Formation of Rodlike Polyelectrolytes. *Physical Review Letters* **82**, 3268-3271 (1999).

6. Perel VI, Shklovskii BI. Screening of a macroion by multivalent ions: a new boundary condition for the Poisson–Boltzmann equation and charge inversion. *Physica A: Statistical Mechanics and its Applications* **274**, 446-453 (1999).

7. Thompson AP*, et al.* LAMMPS - a flexible simulation tool for particle-based materials modeling at the atomic, meso, and continuum scales. *Computer Physics Communications* **271**, 108171 (2022).